Biochar as support in catalytic CO_2 methanation: enhancing effect of CeO_2 addition

Simona Renda[1], Christian Di Stasi[2], Joan J. Manyà[2], Vincenzo Palma[1]*

[1] University of Salerno, Department of Industrial Engineering, Via Giovanni Paolo II 132, 84084 Fisciano (SA), Italy

[2] Aragón Institute of Engineering Research (I3A), Thermochemical Processes Group, University of Zaragoza, Technological College of Huesca, Crta. Cuarte s/n, 22071 Huesca, Spain

* Corresponding author: srenda@unisa.it

Abstract

Biochar obtained through slow pyrolysis was chosen as support in the synthesis of low Ni-content catalysts to be employed in CO_2 methanation process. The main aim of this work was to obtain a more sustainable catalytic formulation compared to those proposed in literature. Biochar-supported catalyst resulted to be efficient in CO_2 methanation, but with a relatively low selectivity toward methane. Support doping with CeO_2 led to a remarkable increase in methane yield and in stability overtime. A maximum CH_4 production was achieved with a CeO_2 loading of 30 wt.%. Nevertheless, the lowest deactivation rate was observed for a support loaded with 50 wt.% of CeO_2 Ceria promotes a faster activation of the CO_2 molecule and a strengthens the Ni/support interactions, resulting in reduced active phase mobility and moderate sintering phenomena. The outcomes of this work were attractive for further studies related to the improvements in the catalyst stability.

Keywords

CO_2 methanation; biochar-based catalysts; catalyst stability; sintering; ecological catalyst

1 Introduction

Catalytic CO_2 methanation is widely recognized as an emergent technology with a key role in the perspective of a carbon-free future scenario. It is at the basis of the Power-to-Gas technology, a flexible solution to convert the off-production of electricity in a valuable gas, methane [1,2]. The reaction, reported in Eq. (1), involves the conversion of hydrogen and carbon dioxide into a methane-rich gas, which is conventionally addressed as synthetic natural gas (SNG).

$$CO_2 + 4H_2 \rightleftarrows CH_4 + 2H_2O \qquad \Delta H_{298K} = -165\ kJ\ mol^{-1} \qquad (1)$$

The positive environmental impact of this process is appreciable from two distinct points of view: from one side, it allows the exploitation of the most abundant pollutant in the atmosphere, carbon dioxide [3,4]; from another side, it represents a technique to store the surplus energy coming from renewable sources [5,6]. Indeed, fluctuations of power generation in renewable sources power plants must be balanced in order to avoid shock overflows of electricity, and energy accumulation systems are becoming the prevalent solution to avoid such issue [7,8]. Hydrogen production via water electrolysis is considered one of the most promising storage technologies and its further conversion into SNG allows its usage in natural gas end-use appliances [9,10].

Based on the above, there are evidence that CO_2 methanation could be a suitable way for the resolution of several environmental issues. Therefore, in recent years the research showed a deep focus in the study of this process. Plenty of catalytic formulations have been proposed so far. As widely recognized, nickel represents the most promising active species to catalyze this reaction, as it offers a good compromise between final cost and catalytic performances. The choice of an adequate support plays a key role in the efficiency of the catalyst [11,12]. Metal oxides with basic properties are particularly suitable as they contribute to CO_2 activation. Furthermore, doping of supports characterized by low oxygen mobility with ions as Zr or Ce is able to enhance the catalysts activity and stability [13,14].

Considering the poor sustainability of the most conventional formulations [15], the research of new and more environmentally friendly alternative is a captivating topic in this field. An almost unexplored route is the employment of selected carbon-based materials as support. In literature, very few works reported the study of CO_2 methanation in presence of carbonaceous materials. Studies on crystalline structures such as carbon nanotubes or nanofibers [16,17] suggest the inactivity of CNTs toward CO_2 activation, and the need of promoters for the obtainment of a sensible catalytic activity. Commercial activated carbons (AC) were found to be more suitable for this application, probably because of their amorphous structure, even if the promoting effect of other components is determining [18,19]. Nevertheless, crystalline carbon structures encounter expensive and non-sustainable production processes, while activated carbons have as main drawback their principal source, which is coal [20,21]. A valid route to the production of more sustainable catalysts can be found in biochar [22]. It is a biomass derived material, conveniently produced via slow pyrolysis [23] and its derivation from biological wastes makes it a more ecological alternative to conventional activated carbons [24]. It has a relatively low price [25] and it can be pretreated and functionalized in order to obtain specific functional groups, high specific surface area or textural properties [26].

The employment of biomass pyrolysis derived biochar as catalyst support for CO_2 methanation has been even less investigated, but the results available in literature are promising. In particular, activated biochars obtained through fast pyrolysis were investigated under conditions of CO methanation [27] and simultaneous CO and CO_2 methanation [28], while CO_2 methanation was studied in presence of modified biochars obtained through slow pyrolysis [29,30]. In these works, doped-biochars were directly produced through pyrolysis of biomass in presence of the doping agent (N or Ce). If projected to industrial scale processes, this would lead to a dedicated production for each catalyst, increasing the costs. On the other hand, it would be more interesting to produce biochar-derived materials (in this case, doped-biochar supports) as value-added products. In this way, biochar functionalization can be treated as separate step from its production and activation, which can be both developed on greater scale.

Based on the above, carbonaceous materials are gaining an increasing interest, but very few and only preliminary investigations have been carried out until now. Furthermore, there is no mention to the stability of the investigated catalysts, which is a truly key aspect in the perspective of transferring the laboratory-scale evaluations to the industrial world; it is also a determining parameter considering that biochar-based catalysts employed in other processes do not offer a high stability over time [31].

This work aims to establish a starting point for a detailed study about the feasibility of employing biomass-derived biochar as catalyst support for CO_2 methanation, considering the activity, selectivity and the stability of the proposed formulations. In this view, this paper reports the investigation of a biochar-supported Ni catalyst in different operating conditions and the feasibility of promoting biochar with ceria, through a series of biochar-CeO_2 supported Ni catalysts for which the effect of CeO_2 addition has been evaluated.

2 Experimental section

For this study, Ni-based catalysts were prepared on activated biochar (BC) and ceria-doped activated biochar (BCCe). A ceria-supported catalyst was also prepared as reference. All the formulations contained 10 wt.% of nickel [32] and a variable CeO_2 loading (i.e., 10, 30 and 50 wt.%). Ni loading is referred to the final formulation, following eq. (2), while CeO_2 loading was considered with respect to the support only, as eq. (3). They are labelled as BCNi and BCNiCeX, as Ni loading was always constant for all the samples and X represents the CeO_2 loading in the support; ceria supported catalyst is labelled as $NiCeO_2$.

$$Ni\,wt.\% = \frac{Ni[g]}{Ni[g]+BC[g]+CeO_2[g]} \qquad (2)$$

$$CeO_2\,wt.\% = \frac{CeO_2[g]}{BC[g]+CeO_2[g]} \qquad (3)$$

2.1 Catalysts preparation

Biochar employed in this work was produced via pyrolysis of wheat straw pellets (9 mm OD and 10-13 mm long) and subsequently activated with CO_2 following a previously optimized procedure. Slow pyrolysis of the raw material was conducted in a fixed bed reactor in N_2 atmosphere at 0.1 MPa and 500°C with a heating rate of 5°C/min [23]. Then, pristine biochar was grounded and sieved (0.12-1.41 mm) and physically activated in CO_2 atmosphere at 700°C and 1.0 MPa [33]. Activated biochar was employed as such in BCNi catalyst and for the preparation of the CeO_2-doped biochar support (BCCe); commercial CeO_2 provided by Rhodia was employed in $NiCeO_2$ sample preparation. BCCe supports were prepared via wet impregnation in aqueous solution. The amount of precursor salt was calculated in order to obtain 10, 30 and 50 wt% of CeO_2. Calcination was performed at 500°C in Ar atmosphere. Nickel was deposited on BC, BCCe supports and CeO_2 (calcined in air at 500°C) via wet impregnation. For the impregnations, $Ni(NO_3)_2{\cdot}6H_2O$ and $Ce(NO_3)_3{\cdot}6H_2O$ (Strem Chemicals) were used as precursor salts.

2.2 Characterization

Textural properties of the prepared catalysts were obtained through N_2 dynamic adsorption/desorption experiments performed at -196°C with an ASAP 2020 automatic adsorption analyzed (Micromeritrics, USA). Samples were degassed in vacuum condition at 150°C. The software MicroActive was employed to determine the following calculations: specific surface area (S_L) value was retrieved using Langmuir model; the total pores volume (V_{tot}) was calculated from the total N_2 adsorbed at high relative pressure (0.99); t-plot method was employed for the calculation of the specific volume of micropores (V_{micro}); non-local density functional theory (NLDFT) and slit-pore geometry were adopted to evaluate the pore size distribution, which allowed the estimation of the mesopores volume (V_{meso}); BJH method was employed for the calculation of the average micro- and mesopores dimension. Temperature programmed reduction (TPR) analysis was performed *in-situ* and constituted also the catalysts activation procedure: a reducing stream (5% H_2 in Ar) was fed to the catalyst; the temperature was increased from room temperature up to 500°C with a heating rate of 5°C/min. The Raman spectra of the fresh and spent catalysts were obtained using an inVia Raman Microscope (Renishaw, Pianezza, Italy), equipped with a 514 nm Ar ion laser operating at 25 mW in the range 100-3200 cm^{-1} Raman shift. At least five measurements were performed for each sample. TEM images were obtained with a Tecnai F20 microscope (FEI, USA). Separation of the particles for the analysis was achieved by sonicating the samples in an ethanol aqueous solution for 5 min.

2.3 CO_2 methanation tests

Experiments were conducted in presence of 1 g of catalyst (particle size <250 μm) diluted with quartz spheres (500÷710 μm) up to a total volume of 3 cm^3. The detailed description of the overall laboratory setup is given elsewhere [34]. The product stream was analyzed continuously by means of a Hiden Analytical mass spectrometer.

For all the experimental tests conducted, the operating absolute pressure was set to 0.1 MPa and the reactants were fed in stoichiometric ratio H_2:CO_2 = 4:1. A dilution ratio of 1:1 reactants:inert was chosen in order to minimize the temperature increase due to the exothermicity of the reaction, resulting in a feed ratio H_2:CO_2:Ar = 4:1:5. Weight-basis gas hourly space velocity (wGHSV, defined as the ratio between the hourly volumetric flow rate and the mass of catalyst employed in the test) was varied in the range 6 to 60 $NL(hg)^{-1}$. For the comparative study of the different formulations, a wGHSV of 6 $NL(hg)^{-1}$ was chosen as preferential operating condition. Activity tests were performed rising the temperature from 200 to 450°C in steps of 25°C. Stability time-on-stream tests were performed at 450°C for 15 h.

Reaction performances were evaluated in terms of CO_2 conversion, CH_4 yield and CO yield, respectively defined as equations (4), (5), (6), (7) and (8), where F_i represents the molar flowrate of the *i*-species. For the stability tests, the half-life of methane yield, t_{half}, was defined as eq. (9), and the deactivation of the catalysts was evaluated from the percentual reduction in methane yield as in equation (10).

$$X_{CO_2} = \frac{F_{CO_2,in} - F_{CO_2,out}}{F_{CO_2,in}} \cdot 100\% \qquad (4)$$

$$Y_{CH_4} = \frac{F_{CH_4}}{F_{CO_2,in}} \cdot 100\% \qquad (5)$$

$$Y_{CO} = \frac{F_{CO}}{F_{CO_2,in}} \cdot 100\% \qquad (6)$$

$$S_{CH_4} = \frac{F_{CH_4}}{F_{CO_2,in} - F_{CO_2,out}} \cdot 100\% \qquad (7)$$

$$S_{CO} = \frac{F_{CO}}{F_{CO_2,in} - F_{CO_2,out}} \cdot 100\% \qquad (8) t_{half} = t\left(\frac{Y^0_{CH4}}{2}\right) \qquad (9)$$

$$\Delta Y^r_{CH_4} = \frac{Y^0_{CH4} - Y^f_{CH4}}{Y^0_{CH4}} \qquad (10)$$

3 Results and Discussion

3.1 Characterization

Textural properties of activated biochar and of the prepared catalysts are reported in Table 1. A high specific surface area (S_L) was obtained for activated biochar, which can be attributed to the presence of micropores. Modification of BC with CeO_2 and deposition of Ni led to a general reduction in specific surface area, due to the severe micropores plugging caused by the formation of metal agglomerates. Nevertheless, CeO_2 addition in low concentration led to the obtention of a higher specific surface area, compared to BCNi sample. This result was coherent with the literature, where the enhancing effect of Ce on Ni dispersion was reported in biochar-supported catalysts [35]. Higher amounts of CeO_2 led to a marked decrease in the specific surface area. The total micropores volume (V_{micro}) of BC was remarkably reduced by metals deposition, while there was a general increment in the mesopores volume (V_{meso}). This means that the deposition of metals onto the biochar surface and their rearrangement created new mesopores which could be helpful for the catalytic activity [36,37]. Furthermore, it is possible to observe from the average pore diameter of micro and mesopores (respectively d_μ and d_m) that the micropores average diameter was not modified by the addition of species on the biochar surface. Indeed, one can conclude that a fraction of the micropores is completely plugged from the deposition of either Ni or CeO_2, as demonstrated by the lowering of the microporous volume, but there is no partial blocking of the microporosities. On the other hand, the mesopores average dimension increases with the increase in the CeO_2 loading. This suggests that the arrangement of CeO_2 particles is progressively more similar to the CeO_2 matrix of $NiCeO_2$ sample. A pronounced drop in specific surface area and mesopores volume was observed for the BCNiCe50 catalyst. This result might be attributed to the encapsulation of the biochar support by ceria [38]. Moreover, because of the higher CeO_2 loading compared to the other samples, formation of new mesopores could have been constrained, leading to such remarkably low specific surface area.

Table 1. Textural properties of the prepared samples

Sample	**S_L** $m^2\ g^{-1}$	**V_{micro}** $cm^3\ g^{-1}$	**V_{meso}** $cm^3\ g^{-1}$	**d_μ** nm	**d_m** nm
BC	600	0.200	0.024	1.86	2.88
BCNi	261	0.083	0.027	1.86	3.10
BCNiCe10	375	0.113	0.055	1.88	3.24
BCNiCe30	87	0.023	0.032	1.86	3.29
BCNiCe50	3	0	0.012	-	3.66
$NiCeO_2$	127	0.011	0.124	1.86	3.76

The reduction profiles for all prepared samples are reported in Figure 1. A two-steps reduction of NiO was observed in BCNi sample, which is often reported for biochar-supported catalysts [39]. The support modification with CeO_2 led to remarkable changes in the reduction profiles. The increase in temperature of the β_1-β_2 peaks observed when CeO_2 loading was variated from 0 to 30 wt.% is ascribable to CeO_2 presence on the catalyst surface, which strengthen the Ni interaction with the support; furthermore, a third peak was observed at lower temperatures. This peak, denoted as α, is probably due to Ni-Ce interaction. As widely recognized CeO_2 induces an anticipated Ni reduction; this could be ascribed to two different effects. On one hand, Ni^{2+} incorporation in the CeO_2 lattice with the substitution of Ce^{4+} cations attests the existence of a $Ni_xCe_{1-x}O_2$ solid solution [40], which generates saturated oxygen vacancies. The oxygenated species formed during this process are highly reactive and, therefore, are easily reduced, even at low temperature [41]. On the other hand, weakly interactive NiO could be also present on the catalyst surface [42]. Furthermore, no consistent CeO_2 reduction was observed for BCNiCe10 and BCNiCe30 samples, suggesting that the final activated catalysts present metallic nickel and cerium oxide particles, as expected [43].

The different behavior of the BCNiCe50 sample suggested a dissimilar arrangement of the metallic phases on the biochar surface. The three peaks resulted shifted at lower temperature, and a fourth peak was observed around 500°C. This profile suggested that, because of the remarkably high CeO_2 loading, NiO is mostly bonded to ceria, obtaining a Ni-Ce-C bonding which resulted in a higher reducibility of the active metal. Even though the enhanced reducibility given by CeO_2 addition seemed to have a greater influence (resulting in a downward shift of the reduction temperatures), it is reasonable to think that the strengthening of Ni interaction with the support is achieved also for BCNiCe50 sample. Hence, considering the hypothesis of Ni-Ce-C bonding, it is possible to speculate that CeO_2 covers almost the whole biochar surface, as a core-shell structure. The fourth observed peak could be ascribed to superficial CeO_2 reduction to Ce_2O_3; ceria partial reduction easily occurs in presence of another metal, because of the spillover phenomenon [42]. Furthermore, for BCNiCe50 sample CeO_2 is supported onto biochar, and this enhance its reducibility if compared to the CeO_2 lattice of $NiCeO_2$ sample.

The reduction profile of $NiCeO_2$ sample upholds the discussion. Indeed, Ni interaction with pure CeO_2 led to three reduction peaks as well, but the α peak was divided into two distinguishable α_1 and α_2 peaks, while a single sharp β peak was present. All the reduction peaks were shifted to lower temperatures compared to the BC supported samples, according to literature [44,45]; a wide peak with very low hydrogen consumption was observed around 400°C, which can be attributed to the superficial CeO_2 reduction.

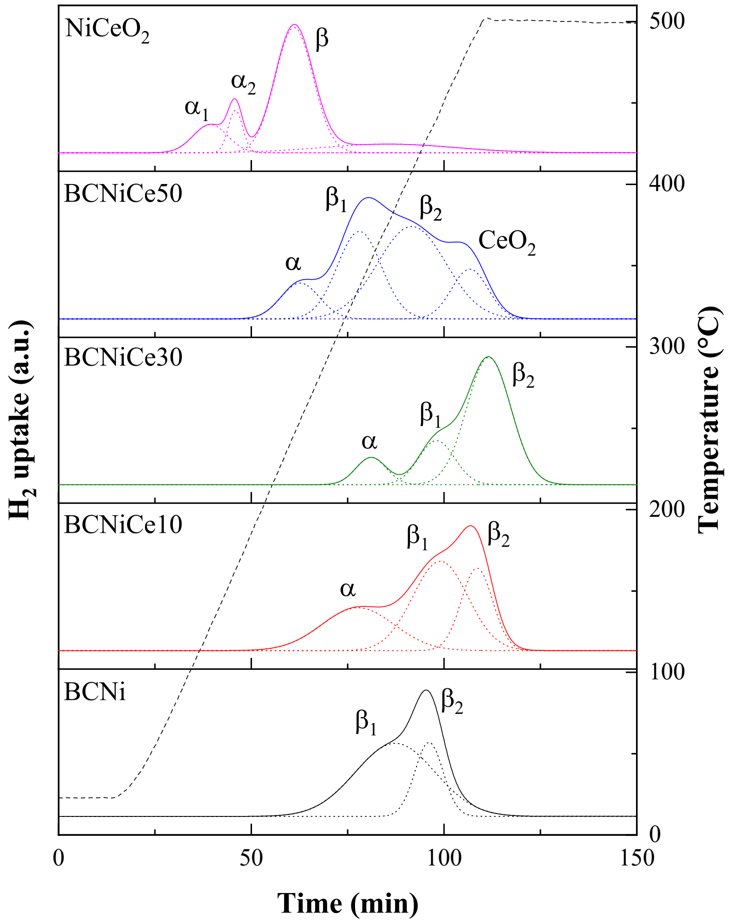

Figure 1. Reduction profiles for the prepared samples: H_2 uptake and temperature vs time

Raman spectra were obtained for the prepared catalysts, activated and pristine biochar, and CeO_2. The complete support Raman characterization is reported in supplementary material. Briefly, the comparison between activated and pristine biochar spectra showed that activation procedure increases the number of defects in biochar structure (Figures S1 and S2, Table S1). These defects could act as active sites for reactants activation and for active species anchorage to biochar surface. For biochar-supported catalysts, the obtained Raman spectra are displayed in Figure 2a, while a comparison with bare CeO_2 and the sample $NiCeO_2$ is given in Figure 2b. CeO_2 shows a main peak at 460 cm^{-1} that is attributed to the first order F_{2g} mode, which corresponds to the Ce^{4+}-O-Ce^{4+} wagging, together with two overlapping peaks ascribable to the defect-induced band (560 cm^{-1}) and Ce^{3+}-O-Ce^{4+} stretching mode (600 cm^{-1}) [46,47]. Supported NiO has a single peak at 550 cm^{-1} [48]; despite the overlapping with the CeO_2 stretching mode and defect-induced bands, it can be easily individuated in the $NiCeO_2$ spectra as broad peak between 550 and 650 cm^{-}

[1]. The presence of NiO is always not detectable in biochar-based catalysts, and even the presence of CeO_2 is not appreciable for the low-loading sample. CeO_2 presence is instead noticeable for BCNiCe30 and BCNiCe50 samples. In particular, for the BCNiCe50 sample the carbon peaks disappear completely, leading to the observance of a full coverage of the biochar support. This is in line with the outcomes of the textural properties analysis and the TPR, from which the hypothesis of encapsulation of biochar was retrieved.

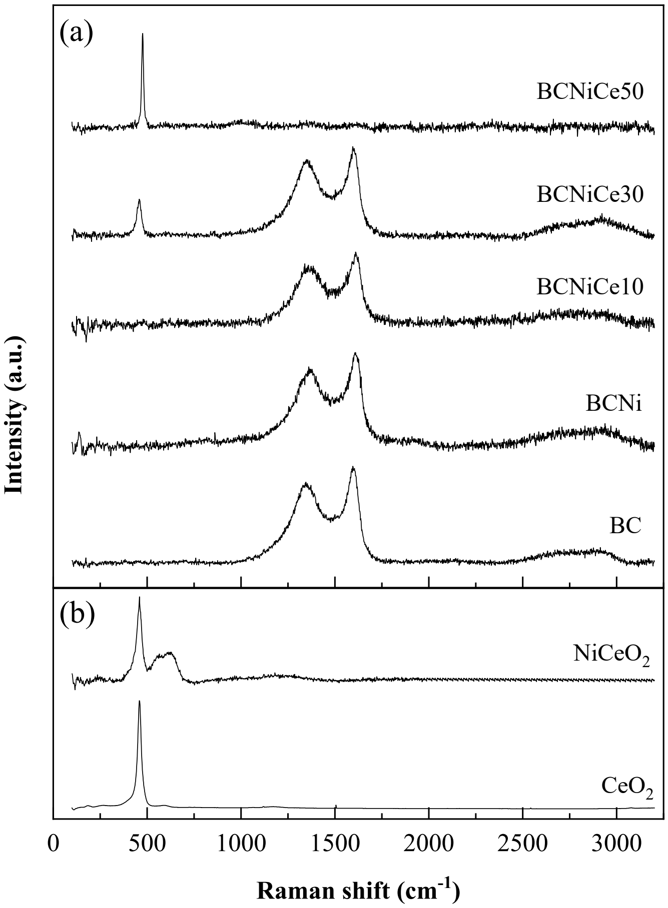

Figure 2. Raman spectra of biochar-supported catalysts and CeO_2 and $NiCeO_2$ samples as comparison

3.2 CO_2 methanation on BCNi: effect of wGHSV

Before starting the experimental campaign, a blank test was conducted on activated biochar. The results (not reported) showed no reactants conversion, thus providing evidence that an appropriate active phase is mandatory to catalyze the reaction. At first instance, the catalytic performances of the BCNi were investigated in a wide range of wGHSVs, spacing from 6 to 60 NL(hg)$^{-1}$. The outcomes are reported in Figure 3. In this reacting system CO_2 methanation and rWGS are competitive reaction, and a variation of the operating conditions such as space velocity or temperature can tune the selectivity of the process. Indeed, together with the impact of wGHSV on the activity, the main aim of this stage was to evaluate the contribution of the catalyst to the desired reaction (CO_2 methanation) and the competitive rWGS reaction. Even though the activity of the catalyst (in terms of CO_2 conversion, Figure 3a) in the three investigated conditions appeared comparable, selective methanation proceeded to remarkably different extent. At high space velocities, the rWGS reaction mainly occurs, as the catalyst demonstrated to have a poor selectivity to methane with a maximum CH_4 yield of 10% obtained at the highest temperature (Figure 3b). Conversely, by decreasing the space velocity to 6 NL(hg)$^{-1}$ it was observed a significant increase in methane yield, which reached the maximum value of 30%. Furthermore, a different behavior was obtained in this latter condition: a maximum in CO yield was observed at 375°C (Figure 3c). Therefore, the combination of low wGHSV and high temperature is able to ensure the increase in selectivity to methane.

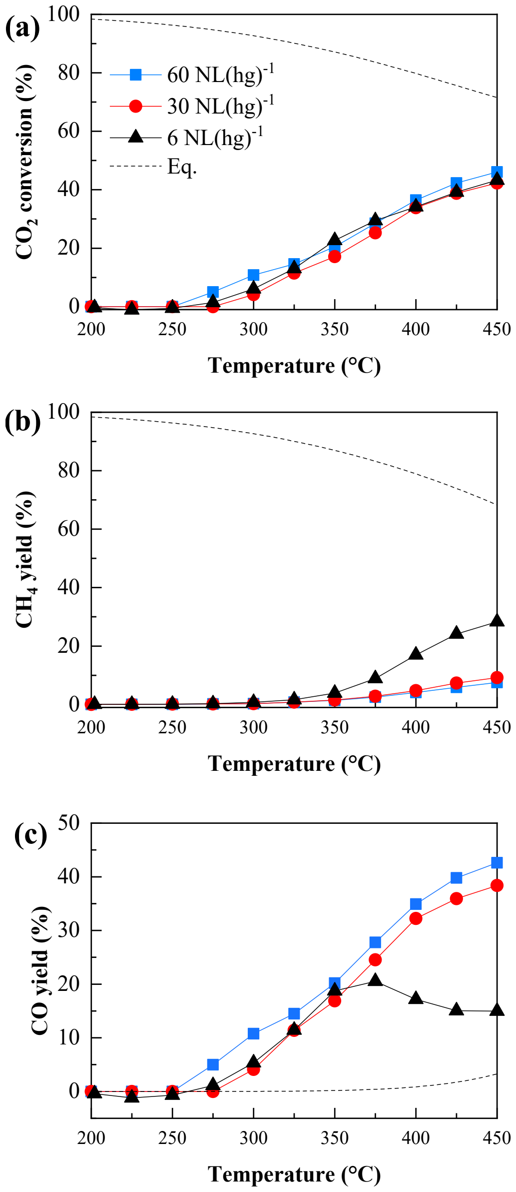

Figure 3. wGHSV influence of reaction performances of the BCNi sample. Operating conditions: P = 0.1 MPa, CO_2:H_2:Ar = 1:4:5.

This suggest that the low selectivity toward methanation can be addressed to a kinetic problem and can be discussed considering the reaction mechanism of catalytic CO_2 methanation. Plenty of studies have been conducted on the topic, leading to the conclusion that methane production occurs following one of two possible pathways: (i) direct CO_2 hydrogenation and (ii) CO_2 conversion to methane with CO formation as reaction intermediate [49]. Despite Ni has been frequently addressed as *methanizer* [50] for its ability to promote direct CO_2 hydrogenation, the consistent CO production and the increase in selectivity to methane experimentally observed at low wGHSV and high temperatures suggest that CO is produced as reaction intermediate and, whereas possible, converted into methane. CO hydrogenation can be addressed as the limiting step of the reaction, considering that high temperatures promote the reaction kinetically and lower space velocities ensures higher contact time for the reaction to occur.

A two-step reaction mechanism has been rarely reported in literature for Ni-based catalysts, nevertheless the occurrence of this pathway might be attributed to the choice of the support. In conventional catalysts, Ni is supported onto metal oxides and a bi-functional mechanism is established [51,52]. Both active metal and support take part to the activation of the reactants, in particular H_2 undergoes chemisorption on the active metal sites and CO_2 is activated at the metal/support interface [53]. This bi-functional mechanism might not occur when biochar is employed as support. If biochar is not able to effectively activate the CO_2 molecule, then this step is demanded to the active metal, already in charge of H_2 activation. CO_2 activation on Ni is particularly difficult because the molecule has to be physically absorbed on the metal site and then could be chemisorbed in a $CO_2^{\delta-}$ state [54]. This complex mechanism might induce Ni to promote an indirect reaction mechanism, with CO formation as reaction intermediate.

In order to provide a component able to efficiently activate CO_2, modification of biochar with CeO_2 was evaluated.

3.3 Effect of CeO_2 doping

BC- and BCCe-supported Ni catalysts were tested under methanation conditions employing a wGHSV of 6 $NL(hg)^{-1}$, which was found to be the optimal value to achieve a significant methanation activity. In addition, a blank test was performed on a selected BCCe support to investigate the eventual contribution of CeO_2 to the catalytic activity; for this evaluation, the sample with 30 wt.% of CeO_2 was employed and labelled as BCCe30. CeO_2 itself is commonly recognized to be not active toward CO_2 methanation, as it can activate CO_2 molecules but, on the other hand, it has a slight interaction with H_2.

Catalytic performances are displayed in Figure 4. As awaited, BCCe30 catalyst showed only rWGS activity. On the other hand, addition of CeO_2 to biochar in any percentage positively contributed to the reaction performances. In fact, all the BCNiCeX samples reported higher conversion values than BCNi in the whole temperature range (Figure 4a). A more important achievement is the improved selectivity toward the desired reaction (Figure 4d). CH_4 yield values increased for all the BCCe supported samples compared to BCNi (Figure 4b), while CO yield (Figure 4c) showed the same non-monotonic trend but, in this case, with consistently lower yield values. Furthermore, the maximum in CO yield, which was observed to be at 375°C for BCNi sample, is shifted toward lower temperatures for all the ceria-doped formulations. This result suggests that CeO_2 co-existence with Ni is able to accelerate both CO and CO_2 methanation reaction. Nevertheless, an optimum in the ceria loading was observed. The increase in CeO_2 loading from 0 to 10 wt.% and from 10 to 30 wt.% determined an overall improvement of the reaction performances, while the further increase from 30 to 50 wt.% caused a worsening of the catalyst activity, leading to lower methane yield. In the whole temperature range, it can be stated that the activity and selectivity of the tested catalysts follows the order BCNiCe30 > BCNiCe10 > BCNiCe50 > BCNi and that the optimal value of CeO_2 loading was 30 wt.%.

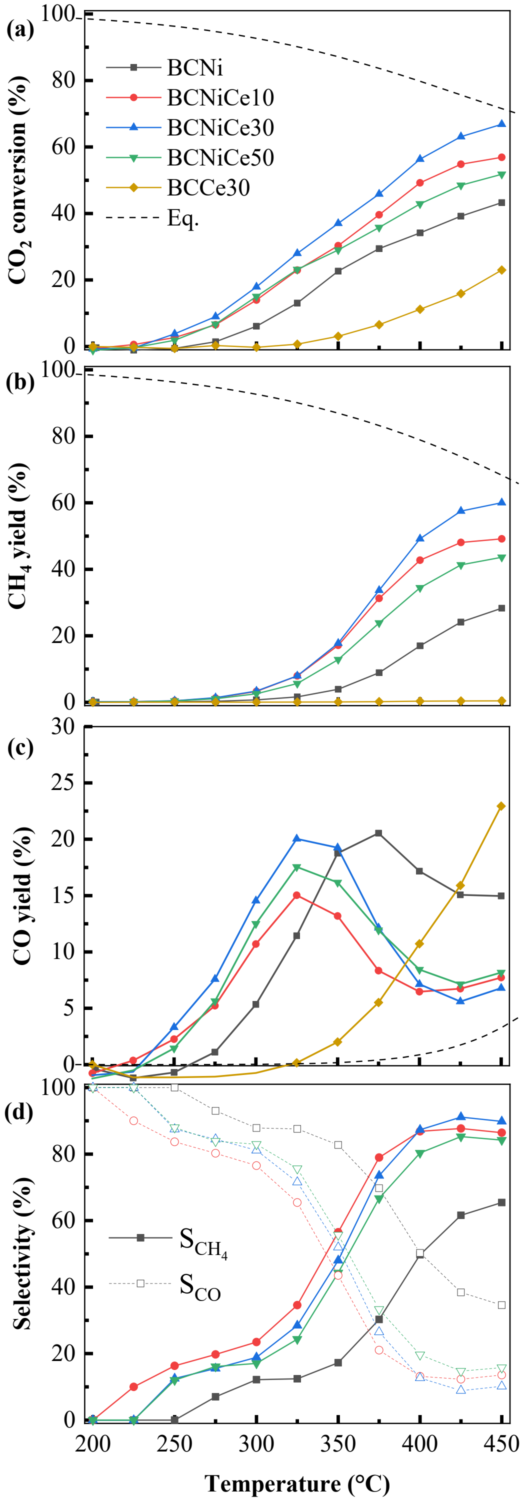

Figure 4. Ce addition and loading effect: activity test results for BCNiCeX and BCCe30 samples. Operating conditions: P = 0.1 MPa, CO_2:H_2:Ar = 1:4:5, wGHSV = 6 NL(hg)$^{-1}$

3.4 Stability tests

The catalysts BCNi and BCNiCeX were tested in a 15 h time-on-stream experiment in order to evaluate their aging stability. The operating conditions for these tests are the same employed for the catalytic activity tests, and the temperature was fixed at 450°C, in order to evaluate the condition in which the maximum methane yield is obtained. BCNi sample demonstrated an almost constant CO_2 conversion (Figure 5a): despite that, it suffered of a strong deactivation that mainly influenced the selectivity. CeO_2 addition, on the other hand, was found to have an enhancing effect on stability as well as on the activity. In fact, together with higher initial CO_2 conversion and CH_4 yield, ceria-doped samples demonstrated to have a lower deactivation rate, resulting in still significant CH_4 yield values at the end of the stability test (Figure 5b). In particular, the deactivation behavior of BCNiCe50 sample was different if compared to the other catalysts. In fact, methane yields for BCNiCe50 sample reached a plateau value at the end of the test, and it appears that in a finite and relatively short time this formulation might ensure the highest methane yield of all the investigates catalysts, despite the initial less favored condition.

In Figure 5c a further analysis of the stability test results is given. The increase in CeO_2 loading in the formulation led to an improvement in both initial and final methane yield. Moreover, the deactivation extent (quantified as Y^r_{CH4}) is progressively lowered by the increase in CeO_2 amount, thus demonstrating that modification of biochar with ceria allows to achieve an increase in the catalyst lifetime. A further evaluation is given related to this latter parameter. In this work, the catalyst was considered deactivated when methane yield reached the 50% of the initial value. Thus, the parameter t_{half} is reported to quantify the half-life of the catalyst. The effect of CeO_2 addition is further highlighted by the significant increase in the catalysts half-life corresponding to the increase in CeO_2 loading in the formulation.

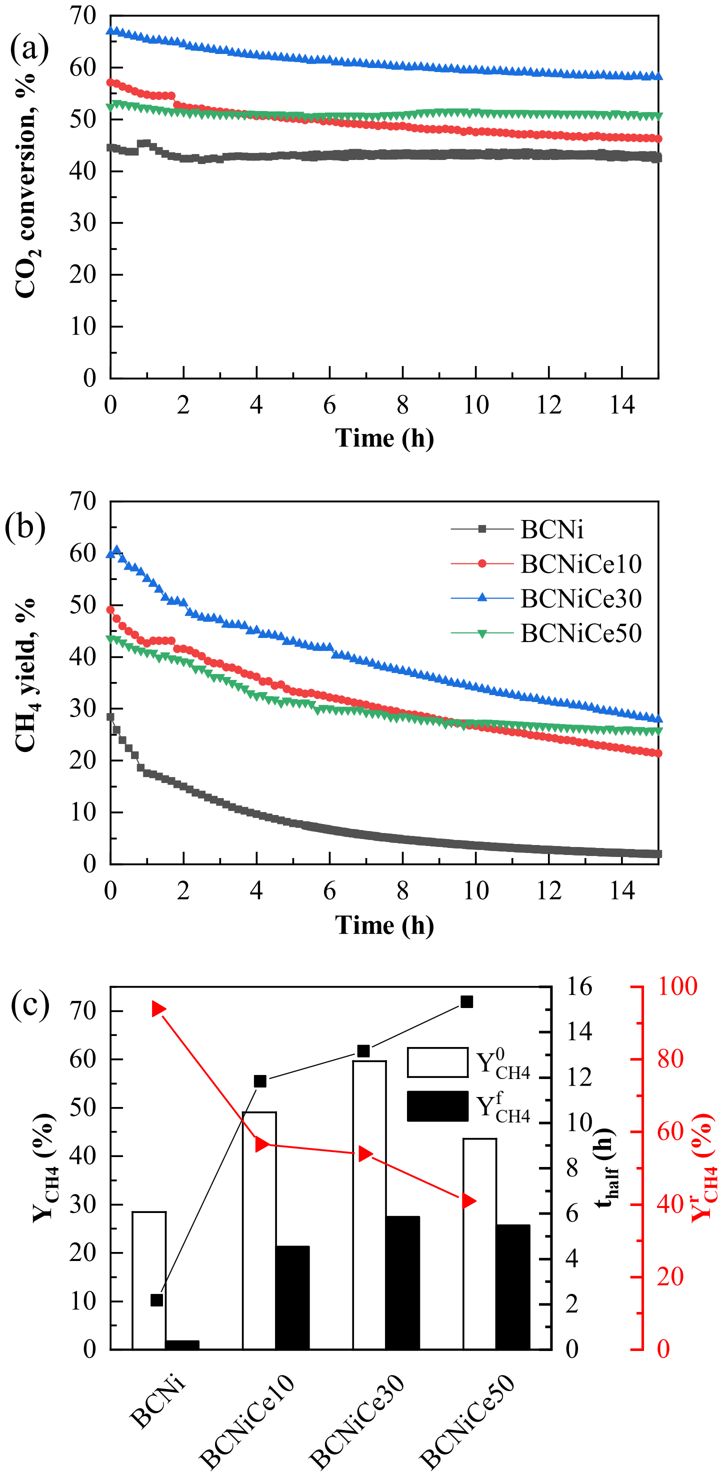

Figure 5. (a, b) Trends of CO_2 conversion and CH_4 yield during the time-on-stream test; (c) Aging stability analysis: $Y_{CH4}{}^0$ and $Y_{CH4}{}^f$ are respectively initial and final yield to CH_4; t_{half} is the half-life of the catalysts; $Y^r{}_{CH4}$ is the reduction in catalytic activity

The higher stability observed for the BCNiCeX formulations compared to BCNi sample can be in general attributed to the strengthening of Ni-support interactions that was also observed by the change in reducibility properties of the bi-metallic samples. Stronger bonds lead to lower Ni mobility and, indeed, higher resistance to sintering. In particular, the observed improved stability of the BCNiCe50 sample can be correlated to the formation of the core-shell structure observed through Raman spectroscopy. The creation of a CeO_2 shell on the biochar surface produced a significant reduction in specific surface area, thus leading to a worse dispersion of the active metal, compared to the other samples: this is likely the reason for the lower catalytic activity of this sample. On the other hand, Ni-CeO_2 interactions are stronger than Ni-biochar ones, and the sintering of the active phase is limited. Indeed, this sample is able to reach a plateau condition within the time of this test. Furthermore, another stabilization mechanism could take place in presence of CeO_2. In fact, ceria is well-known for its oxygen storage capacity, which often plays a key role in catalysts stability limiting the carbonaceous deposits. Nevertheless, recent studies pointed out that oxygen back-spillover could occur from CeO_2 to the active species, leading to the formation of a double layer $[O^{\delta-}\ \delta^{+}]$ which induces electrostatic forces [55]. These forces generate an interparticle repulsion, reducing the tendency to sintering. This mechanism has been observed both for Rh and Ir metal particles supported on ceria-doped metal oxides (gadolinia-ceria or ceria-zirconia), and not in supports with low oxygen ion mobility, such as alumina [56,57].

3.5 Characterization of the spent catalysts

Modifications of the catalysts surface at the end of the stability tests were evaluated through Raman spectra and TEM images of fresh and spent samples. Coke deposition on the catalysts was excluded, as no alteration in the support structure can be observed through the D/G bands ratio in Raman spectra (Figure S3). Moreover, coke deposition is not likely to occur in this system, given the mild operating conditions (low T and P) and the low methane concentration, and the presence of CeO_2 in most of the formulations. Indeed, deposits of solid C have been reported in literature during high-pressure methanation, in which several other reactions take place, forming C2 and C3 hydrocarbons, which easily decompose at low temperature [58]. In addition, carbon deposits formed during CO_2 methanation are often observed as filamentous coke [59–61]. TEM images were obtained for BCNiCe30 and BCNiCe50 samples to further investigate deactivation.

Fresh/spent comparison is given in Figure 6. The presence of filamentous coke was not observed in any of the samples, further endorsing the hypothesis of no coke deposition during the stability test. Instead, for both the samples, a severe sintering occurred, as demonstrated by the visible agglomerations of the metallic phase. The particle size distribution (PSD) shows a significant increment in the particle size for the sample BCNiCe50 (Figure 6e), while the dimension increase for the sample BCNiCe30 is less pronounced (Figure 6f). Nevertheless, it is worth noting that the initial particle size is remarkably different for BCNiCe50 and BCNiCe30 samples, with the former having smaller Ni particles. This outcome further highlights the ability of ceria in promoting the active species dispersion on the catalyst surface. Sintering might be essentially due to two phenomena: support structural collapse or migration of Ni onto the surface, which implies that BC-Ni and Ce-Ni bonding are too weak. Considering the thermal treatment performed on biochar to achieve its activation and the further calcination steps, one can suppose that Ni migration is most likely to occur.

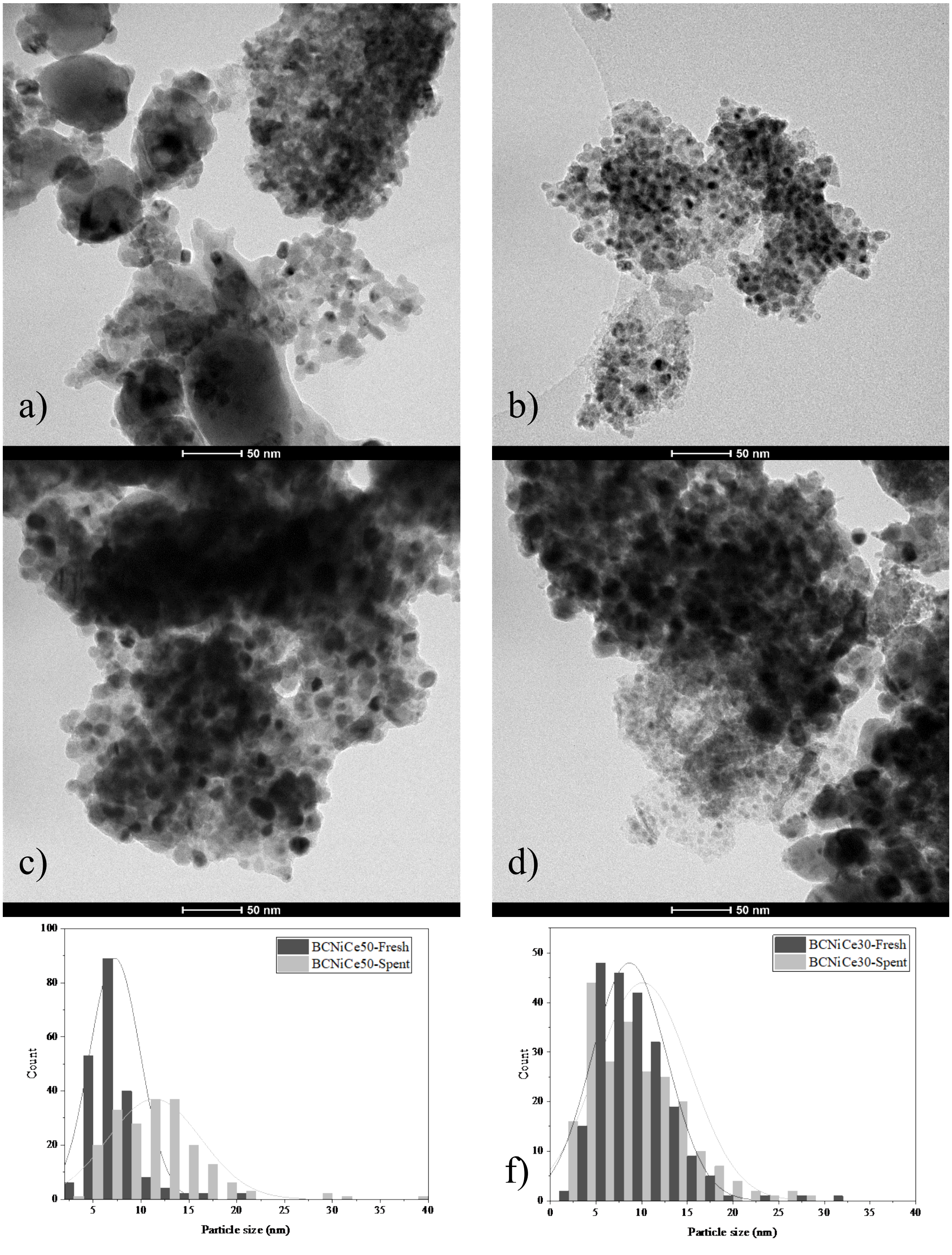

Figure 6. TEM images of BCNiCe50 fresh (a) and spent (c); BCNiCe30 fresh (b) and spent (d); PSD for fresh/spent comparison of BCNiCe50 (e) and BCNiCe30 (f)

4 Conclusions

In this work, activated biochar deriving from slow pyrolysis of wheat straw has been selected as support for catalytic CO_2 hydrogenation to methane. As main outcome, this work pointed out that biochar itself does not participate to the methanation reaction and that, even in presence of a suitable active phase, methanation does not proceed to the desired extent. On the other hand, modification of the support with ceria was crucial for the enhancement of the catalytic performances. In particular, CeO_2 presence was found to be beneficial for both activity and stability of the tested catalysts, as CeO_2 enhances the catalytic performances by promoting CO_2 activation and improves stability by increasing the Ni-support bond strength.

Activity and selectivity of the tested catalysts follows the order BCNiCe30 > BCNiCe10 > BCNiCe50 > BCNi, so that the optimum in Ce loading was found to be 30 wt.%. The presence of an optimal value is due to the pores plugging caused by the excessive loading, which lowered the specific surface area and did not allow an adequate dispersion of the active phase.

Aging stability evaluation pointed out the importance of having the metallic phase strongly bonded to the support: severe Ni sintering was observed, which caused a strong deactivation. Nevertheless, deactivation extent followed the order BCNi > BCNiCe10 = BCNiCe30 > BCNiCe50, demonstrating the importance of CeO_2 presence in reducing the mobility of the active phase.

The optimization of an efficient ecological catalyst might have a consistent scientific relevance in the future scenario. Based on the above, further investigations aimed at stabilizing the metal/support interaction on biochar-based catalysts should be carried out.

References

[1] M. Hervy, J. Maistrello, L. Brito, M. Rizand, E. Basset, Y. Kara, M. Maheut, Power-to-gas: CO_2 methanation in a catalytic fluidized bed reactor at demonstration scale, experimental results and simulation, J. CO2 Util. 50 (2021) 101610. https://doi.org/10.1016/j.jcou.2021.101610.

[2] X. Wang, L. Zhu, Y. Zhuo, Y. Zhu, S. Wang, Enhancement of CO_2 Methanation over La-Modified Ni/SBA-15 Catalysts Prepared by Different Doping Methods, ACS Sustain. Chem. Eng. 7 (2019) 14647–14660. https://doi.org/10.1021/acssuschemeng.9b02563.

[3] Y. Wang, Z. Zhang, S. Zhang, Y. Wang, S. Hu, J. Xiang, X. Hu, Steam reforming of acetic acid over Ni/biochar catalyst treated with HNO_3: Impacts of the treatment on surface properties and catalytic behaviors, Fuel. 278 (2020) 118341. https://doi.org/10.1016/j.fuel.2020.118341.

[4] M. Yang, Z. Lingjun, Z. Xiaonan, R. Prasert, W. Shurong, CO_2 methanation over nickel-based catalysts supported on MCM-41 with in situ doping of zirconium, J. CO2 Util. 42 (2020) 101304. https://doi.org/10.1016/j.jcou.2020.101304.

[5] M. Wolf, L.H. Wong, C. Schüler, O. Hinrichsen, CO_2 methanation on transition-metal-promoted Ni-Al catalysts: Sulfur poisoning and the role of CO_2 adsorption capacity for catalyst activity, J. CO2 Util. 36 (2020) 276–287. https://doi.org/10.1016/j.jcou.2019.10.014.

[6] A. Sternberg, A. Bardow, Life Cycle Assessment of Power-to-Gas: Syngas vs Methane, ACS Sustain. Chem. Eng. 4 (2016) 4156–4165. https://doi.org/10.1021/acssuschemeng.6b00644.

[7] P. Straka, A comprehensive study of Power-to-Gas technology: Technical implementations overview, economic assessments, methanation plant as auxiliary operation of lignite-fired power station, J. Clean. Prod. 311 (2021) 127642. https://doi.org/10.1016/j.jclepro.2021.127642.

[8] L. Karam, M.C. Bacariza, J.M. Lopes, C. Henriques, J. Reboul, N. El Hassan, P. Massiani,

Mesoporous nickel-alumina catalysts derived from MIL-53(Al) metal-organic framework: A new promising path for synthesizing CO_2 methanation catalysts, J. CO2 Util. 51 (2021) 101651. https://doi.org/10.1016/j.jcou.2021.101651.

[9] H.L. Huynh, W.M. Tucho, X. Yu, Z. Yu, Synthetic natural gas production from CO_2 and renewable H_2: Towards large-scale production of Ni–Fe alloy catalysts for commercialization, J. Clean. Prod. 264 (2020) 121720. https://doi.org/10.1016/j.jclepro.2020.121720.

[10] C.I. Melo, D. Rente, M. Nunes Da Ponte, E. Bogel-ŁUkasik, L.C. Branco, Carbon Dioxide to Methane Using Ruthenium Nanoparticles: Effect of the Ionic Liquid Media, ACS Sustain. Chem. Eng. 7 (2019) 11963–11969. https://doi.org/10.1021/acssuschemeng.8b06877.

[11] G.I. Siakavelas, N.D. Charisiou, A. AlKhoori, S. AlKhoori, V. Sebastian, S.J. Hinder, M.A. Baker, I. V. Yentekakis, K. Polychronopoulou, M.A. Goula, Highly selective and stable Ni/La-M (M=Sm, Pr, and Mg)-CeO2 catalysts for CO_2 methanation, J. CO2 Util. 51 (2021) 101618. https://doi.org/10.1016/j.jcou.2021.101618.

[12] G.I. Siakavelas, N.D. Charisiou, S. AlKhoori, A.A. AlKhoori, V. Sebastian, S.J. Hinder, M.A. Baker, I. V. Yentekakis, K. Polychronopoulou, M.A. Goula, Highly selective and stable nickel catalysts supported on ceria promoted with Sm_2O_3, Pr_2O_3 and MgO for the CO_2 methanation reaction, Appl. Catal. B Environ. 282 (2021) 119562. https://doi.org/10.1016/j.apcatb.2020.119562.

[13] F. He, J. Zhuang, B. Lu, X. Liu, J. Zhang, F. Gu, M. Zhu, J. Xu, Z. Zhong, G. Xu, F. Su, Ni-based catalysts derived from Ni-Zr-Al ternary hydrotalcites show outstanding catalytic properties for low-temperature CO_2 methanation, Appl. Catal. B Environ. 293 (2021) 120218. https://doi.org/10.1016/j.apcatb.2021.120218.

[14] Q. Liu, H. Dong, In Situ Immobilizing Ni Nanoparticles to FDU-12 via Trehalose with Fine Size and Location Control for CO_2 Methanation, ACS Sustain. Chem. Eng. 8 (2020) 2093–2105. https://doi.org/10.1021/acssuschemeng.9b07004.

[15] X. Liu, L. Dai, Carbon-based metal-free catalysts, Nat. Rev. Mater. 1 (2016). https://doi.org/10.1038/natrevmats.2016.64.

[16] J.H. Kwak, L. Kovarik, J. Szanyi, Heterogeneous catalysis on atomically dispersed supported metals: CO_2 reduction on multifunctional Pd catalysts, ACS Catal. 3 (2013) 2094–2100. https://doi.org/10.1021/cs4001392.

[17] M. Romero-Sáez, A.B. Dongil, N. Benito, R. Espinoza-González, N. Escalona, F. Gracia, CO_2 methanation over nickel-ZrO_2 catalyst supported on carbon nanotubes: A comparison between two impregnation strategies, Appl. Catal. B Environ. 237 (2018) 817–825. https://doi.org/10.1016/j.apcatb.2018.06.045.

[18] Y. Feng, W. Yang, W. Chu, Effect of Ca modification on the catalytic performance of Ni/AC for CO_2 methanation, Integr. Ferroelectr. 172 (2016) 40–48. https://doi.org/10.1080/10584587.2016.1175333.

[19] C. Swalus, M. Jacquemin, C. Poleunis, P. Bertrand, P. Ruiz, CO_2 methanation on Rh/γ-Al_2O_3 catalyst at low temperature: "In situ" supply of hydrogen by Ni/activated carbon catalyst, Appl. Catal. B Environ. 125 (2012) 41–50. https://doi.org/10.1016/j.apcatb.2012.05.019.

[20] G. Ravenni, G. Cafaggi, Z. Sárossy, K.T. Rohde Nielsen, J. Ahrenfeldt, U.B. Henriksen, Waste chars from wood gasification and wastewater sludge pyrolysis compared to commercial activated carbon for the removal of cationic and anionic dyes from aqueous solution, Bioresour. Technol. Reports 10 (2020) 100421. https://doi.org/10.1016/j.biteb.2020.100421.

[21] S.F. Jiang, L.L. Ling, Z. Xu, W.J. Liu, H. Jiang, Enhancing the Catalytic Activity and Stability of Noble Metal Nanoparticles by the Strong Interaction of Magnetic Biochar Support, Ind. Eng. Chem. Res. 57 (2018) 13055–13064. https://doi.org/10.1021/acs.iecr.8b02777.

[22] S. Wang, H. Li, M. Wu, Advances in metal/ biochar catalysts for biomass hydro-upgrading: A review, J. Clean. Prod. 303 (2021) 126825. https://doi.org/10.1016/j.jclepro.2021.126825.

[23] G. Greco, C. Di Stasi, F. Rego, B. Gonzáles, J.J. Manyà, Effects of slow-pyrolysis conditions on the products yields and properties and on exergy efficiency : A comprehensive assessment for wheat straw, Appl. Energy 279 (2020) 115842.

https://doi.org/10.1016/j.apenergy.2020.115842.

[24] M.T. Moreira, I. Noya, G. Feijoo, The prospective use of biochar as adsorption matrix – A review from a lifecycle perspective, Bioresour. Technol. 246 (2017) 135–141. https://doi.org/10.1016/j.biortech.2017.08.041.

[25] J. Lee, K.H. Kim, E.E. Kwon, Biochar as a Catalyst, Renew. Sustain. Energy Rev. 77 (2017) 70–79. https://doi.org/10.1016/j.rser.2017.04.002.

[26] C. Di Stasi, D. Alvira, G. Greco, B. González, J.J. Manyà, Physically activated wheat straw-derived biochar for biomass pyrolysis vapors upgrading with high resistance against coke deactivation, Fuel 255 (2019) 115807. https://doi.org/10.1016/j.fuel.2019.115807.

[27] L. Zhu, S. Yin, Q. Yin, H. Wang, S. Wang, Biochar: A new promising catalyst support using methanation as a probe reaction, Energy Sci. Eng. 3 (2015) 126–134. https://doi.org/10.1002/ese3.58.

[28] S. Wang, H. Wang, Q. Yin, L. Zhu, S. Yin, Methanation of bio-syngas over a biochar supported catalyst, New J. Chem. 38 (2014) 4471–4477. https://doi.org/10.1039/c4nj00780h.

[29] X. Wang, Y. Liu, L. Zhu, Y. Li, K. Wang, K. Qiu, N. Tippayawong, P. Aggarangsi, P. Reubroycharoen, S. Wang, Biomass derived N-doped biochar as efficient catalyst supports for CO_2 methanation, J. CO_2 Util. 34 (2019) 733–741. https://doi.org/10.1016/j.jcou.2019.09.003.

[30] X. Wang, M. Yang, X. Zhu, L. Zhu, S. Wang, Experimental study and life cycle assessment of CO2 methanation over biochar supported catalysts, Appl. Energy 280 (2020) 115919. https://doi.org/10.1016/j.apenergy.2020.115919.

[31] C. Di Stasi, M. Cortese, G. Greco, S. Renda, B. González, V. Palma, J.J. Manyà, Optimization of the operating conditions for steam reforming of slow pyrolysis oil over an activated biochar-supported Ni e Co catalyst, Int. J. Hydrog. Energy 46 (2021) 26915–26929. https://doi.org/10.1016/j.ijhydene.2021.05.193.

[32] A. Ricca, L. Truda, V. Palma, Innovative catalysts for H_2 conversion to SNG via CO_2 methanation, Chem. Eng. Trans. 70 (2018) 157–162. https://doi.org/10.3303/CET1870027.

[33] C. Di Stasi, G. Greco, R.L.S. Canevesi, M.T. Izquierdo, V. Fierro, A. Celzard, B. González, J.J. Manyà, Influence of activation conditions on textural properties and performance of activated biochars for pyrolysis vapors upgrading, Fuel 289 (2020). https://doi.org/10.1016/j.fuel.2020.119759.

[34] S. Renda, A. Ricca, V. Palma, Study of the effect of noble metal promotion in Ni-based catalyst for the Sabatier reaction, Int. J. Hydrogen Energy 46 (2020) 12117–12127. https://doi.org/10.1016/j.ijhydene.2020.05.093.

[35] M.C. Le, K. Le Van, T.H.T. Nguyen, N.H. Nguyen, The Impact of Ce-Zr Addition on Nickel Dispersion and Catalytic Behavior for CO_2 Methanation of Ni/AC Catalyst at Low Temperature, J. Chem. 2017 (2017). https://doi.org/10.1155/2017/4361056.

[36] L. Xu, X. Lian, M. Chen, Y. Cui, F. Wang, W. Li, B. Huang, CO_2 methanation over Co–Ni bimetal-doped ordered mesoporous Al_2O_3 catalysts with enhanced low-temperature activities, Int. J. Hydrogen Energy 43 (2018) 17172–17184. https://doi.org/10.1016/j.ijhydene.2018.07.106.

[37] F.S. Xiao, Ordered mesoporous materials with improved stability and catalytic activity, Top. Catal. 35 (2005) 9–24. https://doi.org/10.1007/s11244-005-3809-1.

[38] A. Alarcón, J. Guilera, J.A. Díaz, T. Andreu, Optimization of nickel and ceria catalyst content for synthetic natural gas production through CO_2 methanation, Fuel Process. Technol. 193 (2019) 114–122. https://doi.org/10.1016/j.fuproc.2019.05.008.

[39] H.K.D. Nguyen, V. V. Pham, H.T. Do, Preparation of Ni/biochar Catalyst for Hydrotreating of Bio-Oil from Microalgae Biomass, Catal. Letters. 146 (2016) 2381–2391. https://doi.org/10.1007/s10562-016-1873-8.

[40] S. Wang, Q. Pan, J. Peng, T. Sun, D. Gao, S. Wang, CO_2 methanation on $Ni/Ce_{0.5}Zr_{0.5}O_2$ catalysts for the production of synthetic natural gas, Fuel Process. Technol. 123 (2014) 166–171. https://doi.org/10.1016/j.fuproc.2014.01.004.

[41] W. Shan, M. Luo, P. Ying, W. Shen, C. Li, Reduction property and catalytic activity of $Ce_{1-x}Ni_xO_2$ mixed oxide catalysts for CH_4 oxidation, Appl. Catal. A Gen. 246 (2003) 1–9. https://doi.org/10.1016/S0926-860X(02)00659-2.

[42] S. Renda, A. Ricca, V. Palma, Precursor salts influence in Ruthenium catalysts for CO_2

hydrogenation to methane, Appl. Energy 279 (2020) 115767. https://doi.org/10.1016/j.apenergy.2020.115767.

[43] A. Alarcón, J. Guilera, J.A. Díaz, T. Andreu, Optimization of nickel and ceria catalyst content for synthetic natural gas production through CO_2 methanation, Fuel Process. Technol. 193 (2019) 114–122. https://doi.org/10.1016/j.fuproc.2019.05.008.

[44] G. Pantaleo, V. La Parola, F. Deganello, R.K. Singha, R. Bal, A.M. Venezia, Ni/CeO_2 catalysts for methane partial oxidation: Synthesis driven structural and catalytic effects, Appl. Catal. B Environ. 189 (2016) 233–241. https://doi.org/10.1016/j.apcatb.2016.02.064.

[45] C. Tang, B. Sun, J. Sun, X. Hong, Y. Deng, F. Gao, L. Dong, Solid state preparation of NiO-CeO_2 catalyst for NO reduction, Catal. Today. 281 (2017) 575–582. https://doi.org/10.1016/j.cattod.2016.05.026.

[46] V. Palma, E. Meloni, S. Renda, M. Martino, Catalysts for Methane Steam Reforming Reaction: Evaluation of CeO_2 Addition to Alumina-Based Washcoat Slurry Formulation, C — J. Carbon Res. 6 (2020) 52. https://doi.org/10.3390/c6030052.

[47] A. Löfberg, J. Guerrero-Caballero, T. Kane, A. Rubbens, L. Jalowiecki-Duhamel, Ni/CeO_2 based catalysts as oxygen vectors for the chemical looping dry reforming of methane for syngas production, Appl. Catal. B Environ. 212 (2017) 159–174. https://doi.org/10.1016/j.apcatb.2017.04.048.

[48] Y. Wang, G. Xiong, X. Liu, X. Yu, L. Liu, J. Wang, Z. Feng, C. Li, Structure and reducibility of NiO-MoO_3/γ-Al_2O_3 catalysts: Effects of loading and molar ratio, J. Phys. Chem. C. 112 (2008) 17265–17271. https://doi.org/10.1021/jp800182j.

[49] L.M.N.C. Alves, M.P. Almeida, M. Ayala, C.D. Watson, G. Jacobs, R.C. Rabelo-Neto, F.B. Noronha, L. V. Mattos, CO_2 methanation over metal catalysts supported on ZrO_2: Effect of the nature of the metallic phase on catalytic performance, Chem. Eng. Sci. 239 (2021) 116604. https://doi.org/10.1016/j.ces.2021.116604.

[50] K. Yaccato, R. Carhart, A. Hagemeyer, A. Lesik, P. Strasser, A.F. Volpe, H. Turner, H. Weinberg, R.K. Grasselli, C. Brooks, Competitive CO and CO_2 methanation over supported noble metal catalysts in high throughput scanning mass spectrometer, Appl. Catal. A Gen. 296 (2005) 30–48. https://doi.org/10.1016/j.apcata.2005.07.052.

[51] H.Y. Kim, H.M. Lee, J.N. Park, Bifunctional mechanism of CO_2 methanation on Pd-MgO/SiO_2 catalyst: Independent roles of MgO and Pd on CO_2 methanation, J. Phys. Chem. C 114 (2010) 7128–7131. https://doi.org/10.1021/jp100938v.

[52] L. Shen, J. Xu, M. Zhu, Y.F. Han, Essential role of the support for nickel-based CO_2 methanation catalysts, ACS Catal. 10 (2020) 14581–14591. https://doi.org/10.1021/acscatal.0c03471.

[53] C. Sun, P. Beaunier, V. La Parola, L.F. Liotta, P. Da Costa, Ni/CeO_2 Nanoparticles Promoted by Yttrium Doping as Catalysts for CO_2 Methanation, ACS Appl. Nano Mater. (2020). https://doi.org/10.1021/acsanm.0c02841.

[54] H. Chen, M. Yang, J. Liu, G. Lu, X. Feng, Insight into the effects of electronegativity on the H_2 catalytic activation for CO_2 hydrogenation: Four transition metal cases from a DFT study, Catal. Sci. Technol. 10 (2020) 5641–5647. https://doi.org/10.1039/d0cy01009j.

[55] G. Goula, G. Botzolaki, A. Osatiashtiani, C.M.A. Parlett, G. Kyriakou, R.M. Lambert, I. V. Yentekakis, Oxidative thermal sintering and redispersion of Rh nanoparticles on supports with high oxygen ion lability, Catalysts. 9 (2019) 11–15. https://doi.org/10.3390/catal9060541.

[56] I. V. Yentekakis, G. Goula, P. Panagiotopoulou, S. Kampouri, M.J. Taylor, G. Kyriakou, R.M. Lambert, Stabilization of catalyst particles against sintering on oxide supports with high oxygen ion lability exemplified by Ir-catalyzed decomposition of N_2O, Appl. Catal. B Environ. 192 (2016) 357–364. https://doi.org/10.1016/j.apcatb.2016.04.011.

[57] I. V. Yentekakis, G. Goula, S. Kampouri, I. Betsi-Argyropoulou, P. Panagiotopoulou, M.J. Taylor, G. Kyriakou, R.M. Lambert, Ir-Catalysed Nitrous oxide (N_2O) Decomposition: Effect of Ir Particle Size and Metal–Support Interactions, Catal. Letters. 148 (2018) 341–347. https://doi.org/10.1007/s10562-017-2233-z.

[58] T. Franken, A. Heel, Are Fe based catalysts an upcoming alternative to Ni in CO_2 methanation at elevated pressure?, J. CO2 Util. 39 (2020) 101175. https://doi.org/10.1016/j.jcou.2020.101175.

[59] C. Italiano, J. Llorca, L. Pino, M. Ferraro, V. Antonucci, A. Vita, CO and CO_2 methanation over Ni catalysts supported on CeO_2, Al_2O_3 and Y_2O_3 oxides, Appl. Catal. B Environ. 264

(2020) 118494. https://doi.org/10.1016/j.apcatb.2019.118494.

[60] Z. Taherian, A. Khataee, Y. Orooji, Promoted nickel-based catalysts on modified mesoporous silica support: The role of yttria and magnesia on CO_2 methanation, Microporous Mesoporous Mater. 306 (2020) 110455. https://doi.org/10.1016/j.micromeso.2020.110455.

[61] P. Frontera, A. Malara, V. Modafferi, V. Antonucci, P. Antonucci, A. Macario, Catalytic activity of Ni-Co supported metals in carbon dioxides methanation, Can. J. Chem. Eng. 98 (2020) 1924–1934. https://doi.org/10.1002/cjce.23780.